Journal of Crystal Growth 400 (2014) 21–26

Contents lists available at ScienceDirect

Journal of Crystal Growth

journal homepage: www.elsevier.com/locate/jcrysgro

Silver nanostructures formation in porous Si/SiO_2 matrix

Vladimir Sivakov [a,*], Egor Yu. Kaniukov [b], Alexander V. Petrov [b], Olga V. Korolik [c], Alexander V. Mazanik [c], Arne Bochmann [a,d], Steffen Teichert [d], Izabella J. Hidi [e], Alexander Schleusener [a], Dana Cialla [a,e], Maria Eugenia Toimil-Molares [f], Christina Trautmann [f,g], Jürgen Popp [a,e], Sergey E. Demyanov [b]

[a] Leibniz Institute of Photonic Technology, Jena, Germany
[b] Scientific-Practical Material Research Centre of NAS of Belarus, Minsk, Belarus
[c] Belarusian State University, Department of Energy Physics, Minsk, Belarus
[d] Ernst Abbe University of Applied Science, Jena, Germany
[e] Friedrich-Schiller-University, Institute of Physical Chemistry and Abbe Center of Photonics, Jena, Germany
[f] GSI Helmholtz Centre for Heavy Ion Research, Materials Research Department, Darmstadt, Germany
[g] Technische Universität Darmstadt, Darmstadt, Germany

ARTICLE INFO

Article history:
Received 28 February 2014
Received in revised form
18 April 2014
Accepted 21 April 2014
Communicated by K. Deppert
Available online 30 April 2014

Keywords:
A1. Dendrites
A1. Surface processes
A2. Growth from solution
B1. Metals
B2. Magneto-optic materials

ABSTRACT

Self-organized silver nanostructures were grown in porous Si/SiO_2 matrix fabricated by ion track technology. The different silver nanostructures with shapes like "sunflowers", "azalea" or "corn" were realized by applying wet-chemical electroless deposition. We show that reproducible self-organized silver "sunflower" like nanostructures provide a high enhanced Raman signal of Nile blue dye molecules. Signal enhancement for a few or even just a single silver "sunflower" is demonstrated by analyzing the surface-enhanced Raman signature of Nile blue dye molecules. According to this, the silver nanostructures can act as efficient surfaces for surface enhanced Raman spectroscopy as well as (bio)-sensor applications.

1. Introduction

A great deal of effort has been made to fabricate well-defined noble-metal nanostructures such as nanoparticles, nanorods, and nanowires due to their unique optical, electronic, catalytic, and surface-enhanced Raman scattering (SERS) properties [1–5]. A variety of approaches have recently been demonstrated for the shape-controlled synthesis of noble-metal nanostructures because their properties and applications are greatly influenced by their morphology [6].

Dendritic and fractal structures with large surface areas, composed of major trunks and many hierarchical side branches, provide a great opportunity to improve their properties for many different applications. In recent years silver nanostructures have attracted considerable interest due to the relatively low cost and their high electrical conductivity as well as their unique optical, and thermal properties with potential applications in (opto)-electronic devices [7], catalysis [8], and SERS detection [9,10].

SERS is a technique that was developed to detect extremely small quantities of molecules by determining their characteristic Raman signal, i.e. their characteristic vibrational modes [11–16]. The high sensitivity of SERS is mainly due to electromagnetic interaction given by an effective, evanescent field enhancement on the metal surface based on the excitation of surface plasmon-polariton modes. By generating metallic nanostructures with different shapes/dimensions, it is possible to tune the plasmon resonance. Moreover, 3D metallic nanostructures with particularly large active surfaces lead to the increase of the sensitivity since more molecules are adsorbed in the focus area of the laser in comparison to conventional 2D SERS active surfaces.

The intrinsic properties of the metal nanostructures can be tuned by controlling their shape, size, and crystallinity. To date, many approaches have been developed to prepare Ag nanostructures in different shapes, like wires [17–20], belts [21], rice [22], ribbons [23], prisms [24], sheets [25,26], cubes [27], and others [28–32]. Recently, extensive interest has been expressed in the synthesis of more complex hierarchical structures that are ideally composed of nanocrystals (particles, rods, ribbons, sheets, and so

* Correspondence to: Leibniz Institute of Photonic Technology, Albert-Einstein Str. 9, 07745 Jena, Germany. Office: +49 3641206440.
E-mail address: vladimir.sivakov@ipht-jena.de (V. Sivakov).

http://dx.doi.org/10.1016/j.jcrysgro.2014.04.024
0022-0248/

forth) arranged in a particular way as well as their growth mechanism. These types of materials not only possess improved properties originating from their building blocks but also solve the problem of nanomaterial agglomeration. Additionally, they find applications in many fields, especially in (bio)-sensoric technology based on Raman spectroscopy [33,34].

In recent years, the stable growth of costs for developing of new technologies for producing devices composed of very small active elements (down to several nanometers) was observed. Silver nanoparticles [35] and nanowires have been synthesized within a meso-porous template-structured silica [36], self-ordered porous alumina templates [37] or the pores of self-assembled calix-[4]-hydroquinone nanotubes [38].

A prospective approach to the creation of the above mentioned nanodevices is based on the swift heavy ion (SHI) track technology. Ion tracks, created when SHI pass through solids, are known since 1958 [39], and commercially exploited since 1967. The bombardment of materials with SHI produces elongated track regions with different physical and chemical properties than the surrounding matrix material. Each single heavy ion can produce a track of diameter of the order of 10 nm. The irradiation fluence, variable over a wide range from 1 to 10^{10} ion per cm^{-2}, determines the track density. The track distribution across the substrate plane is random, but by means of a mask, tracks can be limited to pre-selected areas [40]. In a second step, the damaged track regions are preferentially etched in a suitable chemical solution where the track is converted into an open pore. The pore shape and size are controlled by the materials properties, irradiation conditions, and the etching process [41,42]. The resulting pore shape depends on the ratio of the track and bulk velocities. In case the track etching rate is much higher than the bulk etching rate, the resulting pore can be regarded as cylindrical, whereas it becomes more conical the smaller the etching rate ratio is. In this way, track-etched pores may have various shapes (cylindrical, conical, etc.) and dimensions from 10 nm up to several μm [42]. In our studies the nanoporous Si/SiO_2 template was formed by chemical etching of the irradiated SiO_2 layer in dilute HF at ambient conditions. Selective etching is based on the fact that track regions contain numerous defects like distorted and broken bonds, point defects, etc. Also, the chemical reactivity of tracks is higher compared with the surrounding matrix material. The resulting pores are characterized by their length (thickness of SiO_2 layer (d_{SiO_2})), and by the top and bottom diameter d_{top} and d_{base}, respectively (Fig. 1).

In this paper we demonstrate the synthesis of Ag hierarchical nanostructures arrays as shown in Fig. 2 consisting of complex but adjustable structures produced by a surfactant-free and rather simple production route under mild conditions. We should mention that only one publication [43] reports on the silver nanowires growth in the etched ion-track polycarbonate membranes.

The ultimate goal of this work is a selective growth of well-defined self-organized silver nanostructures in porous Si/SiO_2 matrix and their SERS spectroscopic characterization. The synthesis consists of three main stages: (i) the irradiation of a Si/SiO_2 surface with swift heavy ions (SHI) leading to the creation of nanometer-sized tracks in the SiO_2 matrix; (ii) wet-chemical etching in diluted hydrofluoric acid (HF), where each ion track is converted into an open nanopore; (iii) growth of nanostructures by electrodless deposition of silver into the nanopores.

2. Experimental part

Single-crystalline phosphorous doped silicon wafers with (100)-orientation (4.5 Ω cm) were used as surfaces for the creation of Si/SiO_2 structures. By the thermal (pyrogenic) oxidation method an amorphous silicon oxide layer with thickness about 700 nm was formed [44]. The Si/SiO_2 wafers were irradiated with 350 MeV gold (^{197}Au) ions. The beam energy was sufficient to completely penetrate through the dielectric SiO_2 layer and produce tracks. The ions are finally stopped in the substrate without forming tracks in the silicon wafer because silicon is insensitive [45]. The irradiations were performed under normal incidence leading to randomly distributed, parallel oriented ion tracks in the SiO_2 layer. The applied ion fluence was adjusted to 10^8 per cm^{-2} which is sufficiently low to avoid severe pore overlapping after track etching. The introduced number of gold atoms is by many orders of magnitude less than the phosphor concentration in the silicon substrate, thus the Au implantation has no influence on the electrical resistivity. The irradiated samples were etched in hydrofluoric (HF) acid resulting in pores down to the Si surface. As described in previous publications [42,46], in SiO_2 the etching rate along ion tracks is about 2.5–3 times higher than the bulk etching rate of non-irradiated regions.

In our experiments, SHI tracks were etched in 2.5% hydrofluoric acid at room temperature for times between 10 and 30 min. After 15 min wet-chemical treatment, pores with frustum geometry (Fig. 3) were formed with an average diameter (top) ~300 nm and height corresponding to the thickness of the SiO_2 layer (~400 nm). After 25 min of etching, the pore diameter was about 800 nm. Scanning electron microscopy (SEM) and energy dispersive X-ray analysis (EDX) of porous templates based on Si/SiO_2 structures are shown in Fig. 2. As described in our previous publication [47], the deposition of metal in track-etched pores makes it also possible to create metal-dielectric-semiconductor structures. A number of unusual electrical–physical phenomena was observed in these structures, including, e.g., the magneto-resistive effect which reaches maximal values in sequential layers of ferromagnetic and para-diamagnetic metals but is not yet well understood.

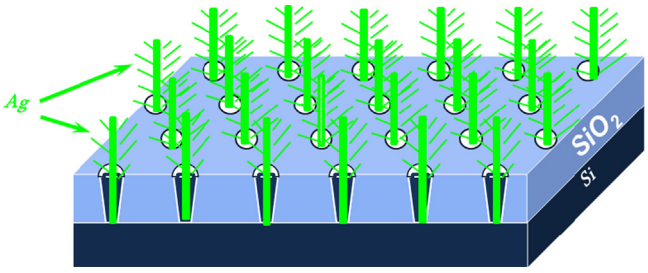

Fig. 2. Schematic cross section view of porous SiO_2 template on Si substrate selectively filled with silver dendritic nanostructures.

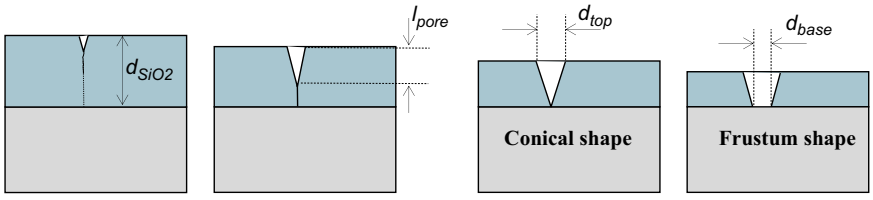

Fig. 1. Schematic cross section view of different stages of etching of a single ion track in a Si/SiO_2 sample.

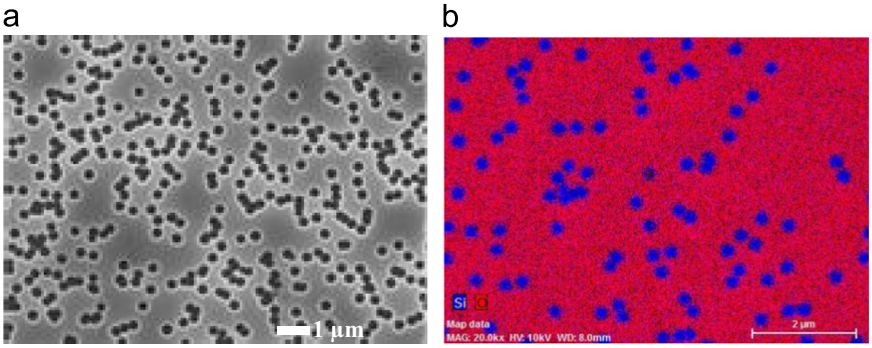

Fig. 3. (a) Planar scanning electron microscopy micrograph and (b) element map (blue: silicon; red: oxygen) from energy dispersive X-ray analysis of a Si/SiO_2 sample irradiated with 350 MeV gold ions and exposed to chemical track etching. (For interpretation of the references to color in this figure legend, the reader is referred to the web version of this article.)

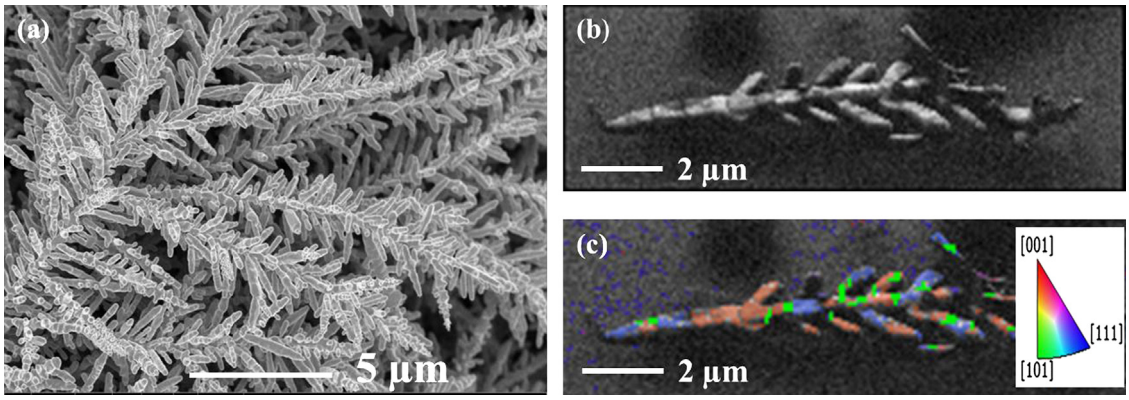

Fig. 4. (a, b) SEM micrographs of silver dendrite nanostructure on n-Si (100) grown for 30 s at atmospheric conditions; (c) EBSD analysis of single silver dendrite; color coded inverse pole figure representation. (For interpretation of the references to color in this figure legend, the reader is referred to the web version of this article.)

Recently, a simple wet-chemical electrodless silver deposition (WCED) [48–51] method was applied using a hydrofluoric acid (HF) solution containing silver nitrate ($AgNO_3$). The procedure is suitable to synthesize unique silver (Ag) dendritic nanostructures with stems, branches, and leaves. WCED in ionic metal (silver) HF solution is based on an electrochemical redox reaction in which both anodic and cathodic processes occur simultaneously at the silicon surface [52]. Ag nanostructures were formed on planar n-Si (100) and SHI irradiated n-Si/SiO_2 surfaces by immersing samples in an aqueous solution of 0.02 M silver nitrate and 5 M HF in the volume ratio 1:1 at room temperature (20 ± 1 °C) for 30 s. Finally, the sample surfaces were rinsed several times in de-ionized water and dried at room temperature.

Structural analysis of the silver nanostructures was carried out by field emission scanning electron microscopy (Carl Zeiss ULTRA 55, FE-SEM). EDX analysis was performed in the specimen chamber of an EDX coupled SEM Bruker XFlash® 6 30 SDD EDS Detector. The growth direction and crystal structure of the silver nanostructures were investigated using Electron Backscatter Diffraction (EBSD) (Bruker e-Flash^{HR} EBSD Detector+ARGUS™ FSE/BSE-Detector System). Combining FE-SEM and EBSD allows the determination of individual grain orientations, local textures, and point to point orientation correlations on bulk surfaces of polycrystalline materials [53,54].

The standard dye molecule like Nile blue was used to study the Raman signal enhancement induced by silver nanostructures in "sunflower" shape. In order to perform SERS measurements, 150 μl 10^{-5} M Nile blue ($C_{20}H_{20}ClN_3O$) of an aqueous solution was dropped on the samples with "sunflowers" nanostructures with incubation time of 15 min, and subsequently rinsed in deionized water, and finally, dried in air. The Raman scattering measurements were performed at room temperature on a Nanofinder High End (Lotis TII, Belarus–Japan) confocal microscope based setup. A solid-state diode laser (wavelength 532 nm) was used as excitation source. The laser power at the samples' surface was kept at 25 μW and the typical single spectrum acquisition time was 10 s. The backscattered light, not analyzed for its polarization, was dispersed using a spectrograph with 0.55 m focal length equipped with a 600 lines/mm single grating spectrometer with a spectral resolution around 3 cm^{-1} and detected by a cooled CCD camera. The laser beam was focused through a "50×" microscope objective lens. The resulting spot diameter was about 1 μm. In order to illustrate the distribution of the Raman signal across the surface, a 20×20 μm^2 square with the step size of 0.2 μm is scanned.

3. Results and discussion

The formation of silver dendrites via galvanic deposition has been reported using bulk materials (e.g., silicon, aluminum, copper, zinc) as substrates [55–59]. In general, the above mentioned method normally involves the reduction of silver salts in the presence of potentiostatic or organic surfactants, at elevated temperature, or requiring the removal of template/substrate to get pure products. Fig. 4 shows typical Ag dendrite nanostructures synthesized by using a mixture of 5 M HF and $AgNO_3$ (0.02 M) in aqueous solution grown for 30 s on non-structured n-Si(100) substrate. The uniformity of a large number of such structures is illustrated in Fig. 4a. The dendrite structures with multilevel generations, having a long main trunk with short side branches (or even further sub-branches), all decorated by small leaves. Generally, the lengths of the trunks and (sub)-branches are several

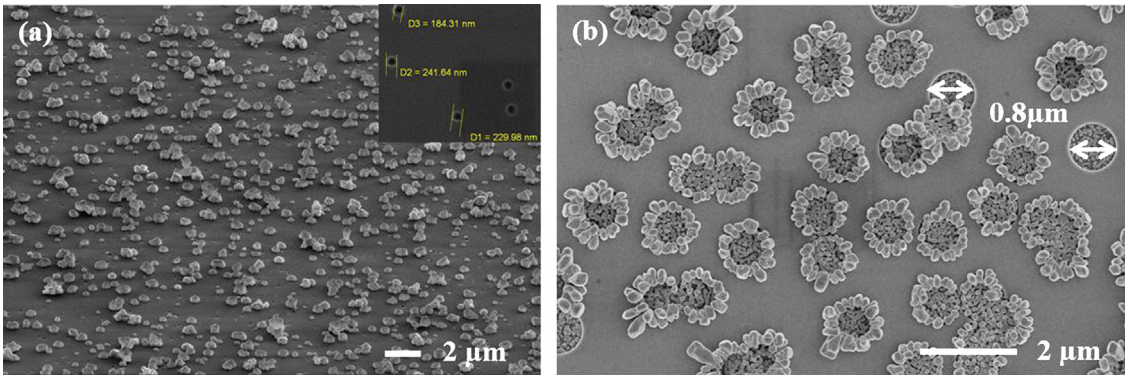

Fig. 5. SEM micrographs of silver nanocrystals selectively grown in pores with average top diameter (a) 200 nm (inset shows pores before Ag deposition) and (b) 800 nm.

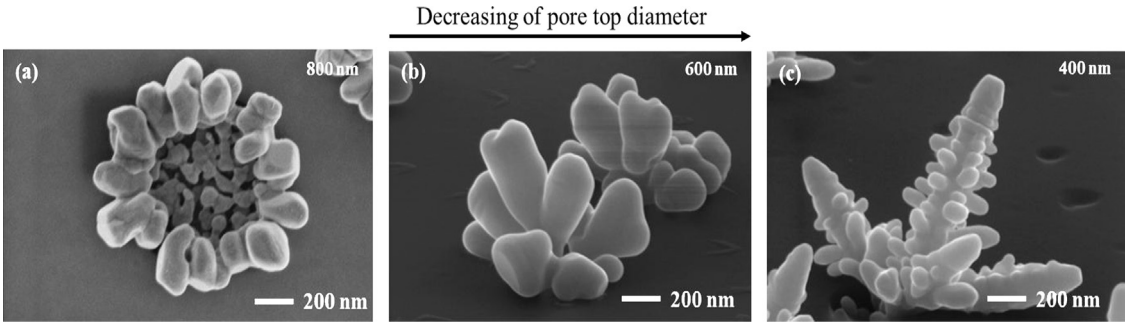

Fig. 6. SEM micrographs of silver nanostructures with (a) "sunflower", (b) "azalea" and (c) "corn"-like shapes.

tens of micrometers and several micrometers, respectively. The diameters of all structures (trunk, branch, and sub-branches) have a similar size of few tens of nanometers.

The crystallinity character of the silver dendrites was investigated by EBSD of spatial resolution of a few 10 nm even over large probed areas allowing orientation analysis with respect to grain size (or single crystallinity), grain distribution, and silver orientations. Fig. 4c gives evidence of single crystallinity of the silver dendrites over the full trunk length and branches with the presence of twins in the branching area.

The evolution of the nanostructure topology was studied to obtain a complete view of the Ag dendrite formation process and its growth mechanism. The pore diameter (top) was changed from approx. 200 to 800 nm by varying the etching time from 10 to 30 min, respectively. The silver formation is based on the galvanic displacement of Si by Ag^+ to Ag^0 reduction on the wafer surface [60]. The reaction proceeds in an aqueous solution of $AgNO_3$ and hydrofluoric acid. Ag^+ reduces onto the Si wafer surface by injecting holes into the Si valence band and oxidizing the surrounding lattice. The initial reduction of Ag^+ forms Ag^0 nanoparticles on the wafer surface. Further reduction of silver occurs on the newly formed nanoparticles, not the Si wafer, which becomes the active cathode by electron transfer from the underlying wafer. Fig. 5 shows SEM images of silver nanostructures grown in 200 and 800 nm wide (top diameter) pores.

The size of the pores strongly influences the morphology of the silver nanostructures. In pores with a top diameter of 200 nm, the growth process yields single silver nanocrystals with little caps, while larger pores (800 nm in top diameter) lead to a totally different morphology with self-organized silver "sunflowers" (Fig. 5b), although the growth conditions were identical (0.02 M silver nitrate and 5 M HF, room temperature; 30 s growth time). Tuning the parameters of the track etching process (e.g., concentration of silver cations in the etching solution, etchant temperature, etc.) produces quite different self-organized and reproducible shapes of "plasmonic nanogarden" objects such as "sunflowers", "corns" or "azaleas" (Fig. 6). The growth mechanism of 3D silver nanostructures in porous matrix can be explained by the numerical calculations of particle trajectory and deposition using FEMLAB program (COMSOL) performed by Lee et al. [61] that corresponds that the column or 3D growth strongly depends on the particles concentration as shown in Fig. 3b–d [61]. In our case it can be explained that concentration of silver particles in pore less than on the surface between the pores that guided to the vertical growth of silver nanoparticles inside the pore, and the hierarchical structures grew atop of pore where concentration of silver nanoparticles is higher and limited by the solution volume. The growth mechanism obviously depends strongly on the pore volume, pore formation (ion mass, energy, fluence) and silver deposition conditions (concentration, solution temperature and growth time) conditions. Detailed studies on the process kinetics and growth mechanism will be discussed in a separate publication.

Fig. 7 shows the SERS spectrum of Nile blue (NB, $C_{20}H_{20}ClN_3O$) molecules obtained from a sample with "sunflower" shaped nanostructures. Prior to the measurement, 150 µl of 10^{-5} M NB solution was dropped on the "sunflowers" surface for 15 min, afterward rinsed in water, and finally dried in the air. Under the excitation with a 532 nm laser light, the "sunflower" shaped silver nanostructures exhibit a high Raman signal as shown in Fig. 7a. Besides the prominent band located at 521 cm^{-1} corresponded to crystalline silicon vibration, in the presented spectrum; all other bands are characteristic Raman modes for the Nile blue molecule. As the "sunflowers" are relatively well-separated, it was possible to monitor the SERS signal of one individual "sunflower" by means of Raman mapping. The mapping was performed by scanning a 20×20 μm^2 square with step of 0.2 µm and monitoring the intensity of the 593 cm^{-1} band (phenoxazine ring mode) of Nile blue (Fig. 7b).

The SERS spectrum obtained from incubating the "sunflower" shaped nanostructures with a diluted NB solution (10^{-5} M) exhibits a high Raman signal intensity giving clear evidence that such silver nanostructures grown in pores of etched SHI tracks are

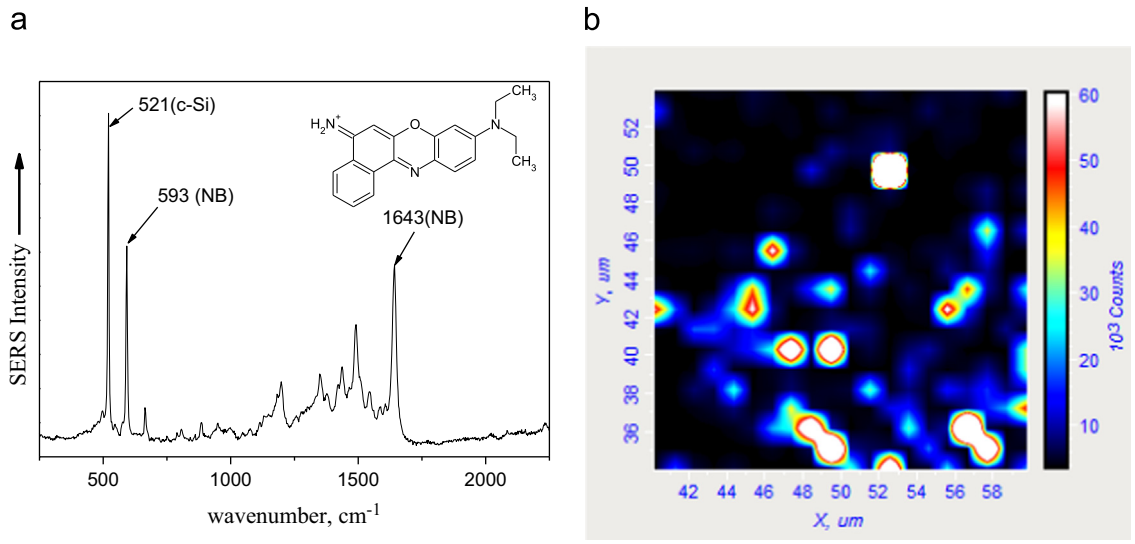

Fig. 7. (a) SERS spectrum of Nile blue (NB) molecules (inset) obtained from a sample with "sunflower" shaped nanostructures; (b) $20 \times 20\ \mu m^2$ map of individual "sunflower" shaped nanostructure showing the intensity of the Raman band at 593 cm^{-1}.

suitable for the Raman enhancement and are promising for broad exploitation for Raman analysis and imaging.

4. Conclusions

In summary, we have for the first time demonstrated a simple method for the formation of silver nanostructures deposited in etched SHI tracks in SiO_2 by applying a WCED. The morphology of these silver nanostructures depends on the volume and diameter of the pores as well as on the growth kinetics (such as concentration of silver salt, growth time, process temperature). The obtained silver nanostructures with "sunflower" shape show SERS sensitivity allowing the detection of Nile blue dye molecules. This indicates that silver nanostructures grown in etched ion tracks are an active substrate for enhancement of Raman signal.

Acknowledgment

This work was supported by the National Science Foundation of Germany (DFG) under Grant no. SI 1893/2-1 and the European FP7 Project "PIRSES-GA-2011–295273-NANEL". The funding of the PhD project of I.J. Hidi within the framework "Carl-Zeiss-Strukturmaßnahme" is gratefully acknowledged. The projects "Quanti-SERS" and "Jenaer Biochip Initiative 2.0" within the framework "InnoProfile Transfer – Unternehmen Region" are supported by the Federal Ministry of Education and Research, Germany (BMBF).

References

[1] Y. Sun, Y. Xia, Science 298 (2002) 2176.
[2] F. Kim, J.H. Song, P.D. Yang, J. Am. Chem. Soc. 124 (2002) 14316.
[3] T. Teranishi, M. Miyake, Chem. Mater. 10 (1998) 594.
[4] D. Cialla, U. Hübner, H. Schneidewind, R. Moller, J. Popp, ChemPhysChem 9 (5) (2008) 758.
[5] R.C. Jin, C.Y. Cao, E.C. Hao, G.S. Metraux, G.C. Schatz, C.A. Mirkin, Nature 425 (2003) 487.
[6] A.R. Tao, S. Habas, P. Yang, Small 4 (2008) 310.
[7] H. Wang, L. Qi, Adv. Funct. Mater. 18 (2008) 1249.
[8] M.A. Kostowskyj, D.W. Kirk, S.J. Thorpe, Int. J. Hydrogen Energy 35 (2010) 5666.
[9] B.J. Wiley, Y. Chen, J. McLellan, Y. Xiong, Z.-Y. Li, D. Ginger, Y. Xia, Nano Lett. 7 (2007) 1032.
[10] S. Nie, S.R. Emory, Science 275 (1997) 1102.
[11] E. Smith, G. Dent, Modern Raman Spectroscopy: A Practical Approach, Wiley, 2005.
[12] K. Kneipp, H. Kneipp, I. Itzkan, R.R. Dasari, M.S. Feld, J. Phys.: Condens. Matter 14 (2002) R597.
[13] D. Cialla, A. März, R. Bohme, F. Theil, K. Weber, M. Schmitt, J. Popp, Anal. Bioanal. Chem. 403 (2012) 27.
[14] S. Pahlow, A. März, B. Seise, K. Hartmann, I. Freitag, E. Kämmer, R. Bohme, K. Weber, D. Cialla, J. Popp, Eng. Life Sci. 12 (2012) 131.
[15] H. Kneipp, N. Mobjerg, A. Jorgensen, H.G. Bohr, C. Helix-Nielsen, J. Kneipp, K. Kneipp, J. Biophotonics 6 (10) (2013) 759.
[16] N. Pavillon, K. Bando, K. Fujita, N.I. Smith, J. Biophotonics 6 (8) (2013) 587.
[17] X. Sun, Y. Li, Adv. Mater. 17 (2005) 2626.
[18] J. Fang, H. Hahn, R. Krupke, F. Schramm, T. Scherer, B. Ding, X. Song, Chem. Commun. 9 (2009) 1130.
[19] J. Liu, C. Tsai, Y. Chiu, F. Hsieh, Nanotechnology 20 (2009) 035301.
[20] T.D. Lazzara, G.R. Bourret, R.B. Lennox, T.G.M. van de Ven, Chem. Mater. 21 (2008) 2020.
[21] B. Liu, X. Zhao, Mater. Res. Bull. 44 (2009) 682.
[22] H. Liang, H. Yang, W. Wang, J. Li, H. Xu, J. Am. Chem. Soc. 131 (2009) 6068.
[23] C. Marchal-Roch, C.M. Mayer, A. Michel, E. Dumas, F.X. Liu, F. Sechersse, Chem. Commun. 36 (2007) 3750.
[24] J. Zhang, H. Liu, P. Zhan, Z. Wang, N. Ming, Adv. Funct. Mater. 17 (2007) 1558.
[25] G. Liu, W. Ci, C. Liang, Cryst. Growth Des. 8 (2008) 2748.
[26] J. Yang, H. Wang, H. Zhang, J. Phys. Chem. C 112 (2008) 13065.
[27] S.E. Skrabalak, L. Au, X. Li, Y. Xia, Nat. Protoc. 2 (2007) 2182.
[28] B.K. Jena, B.K. Mishra, S. Bohidar, J. Phys. Chem. C 113 (2009) 14753.
[29] X. Liu, F. Zhang, R. Huang, C. Pan, J. Zhu, Cryst. Growth Des. 8 (2008) 1916.
[30] M. Baia, L. Baia, S. Astilean, J. Popp, Appl. Phys. Lett. 88 (14) (2006) 143121.
[31] W.C. Zhang, X.L. Wu, H.T. Chen, Y.J. Gao, J. Zhu, G.S. Huang, P.K. Chu, Acta Mater. 56 (2008) 2508.
[32] K.K. Hering, R. Moller, W. Fritzsche, J. Popp, ChemPhysChem 9 (6) (2008) 867.
[33] M. Salehi, D. Steinigeweg, Ph. Strobel, A. Marx, J. Packeisen, S Schlücker, J. Biophotonics 6 (10) (2013) 785.
[34] P. Negri, R.A. Dluhy, J. Biophotonics 6 (1) (2013) 20.
[35] Y. Sun, Y. Xia, Science 298 (2002) 2176.
[36] Y. Plyuto, J.-M. Berquier, C. Jacquioda, Ch. Ricolleau, Chem. Commun. 17 (1999) 1653.
[37] G. Sauer, G. Brehm, S. Schneider, K. Nielsch, R.B. Wehrspohn, J. Choi, H. Hofmeister, U. Gosele, J. Appl. Phys. 91 (5) (2002) 3243.
[38] B.-H. Hong, S.-C. Bae, C.-W. Lee, S. Jeong, K.S. Kim, Science 294 (2002) 348.
[39] R.L. Fleischer, P.B. Price, R.M. Walker, Nuclear Tracks in Solids, University of California Press, Berkeley, 1975.
[40] A. Razpet, G. Possnert, A. Johansson, et al., J. Appl. Phys. 97 (2005) 44310.
[41] D. Fink, P.S. Alegaonkar, A.V. Petrov, et al., Nucl. Instrum. Methods B 236 (2005) 11.
[42] Yu.A. Ivanova, D.K. Ivanou, A.K. Fedotov, E.A. Streltsov, S.E. Demyanov, A.V. Petrov, E.Yu. Kaniukov, D Fink, J. Mater. Sci 42 (2007) 9163.
[43] H.-J. Yao, J. Liu, J.-L. Duan, M.-D. Hou, Y.-M. Sun, D. Mo, Y.-F. Chen, Z.-H. Xue, Acta Phys. Chim. Sin. 23 (4) (2007) 489.
[44] N.V. Rumak, Nauka Tekh. 190 (1986) (in Russian).
[45] C. Trautmann, Ion Beams in Nanoscience and Technology, R. Hellborg et al. (Eds.), 2009, p. 369.
[46] D. Fink, Fundamentals of Ion-Irradiated Polymers Springer Series in Materials Science, vol. 63, 2004, p. 391.
[47] S.E. Demyanov, E.Yu. Kaniukov, A.V. Petrov, V. Sivakov, Sens. Actuators A (2014), in press.
[48] K.Q. Peng, Y.J. Yan, S.P. Gao, J. Zhu, Adv. Mater. 14 (2002) 1164.
[49] V. Sivakov, F. Voigt, B. Hoffmann, V. Gerliz, S. Christiansen, Nanowires – Fundamental Research, InTech (2011), pp. 45–80 (Chapter 3).

[50] T. Qiu, X.L. Wu, Y.F. Mei, P.K. Chu, G.G. Siu, Appl. Phys. A 81 (2005) 669.
[51] V. Sivakov, S. Christiansen, J. Nanoelectron. Optoelectron. 7 (2012) 583.
[52] P. Gorostiza, M.A. Kulandainathan, R. Diaz, F. Sanz, P. Allongue, J.R. Morante, J. Electrochem. Soc. 14 (2000) 1026.
[53] A.J. Schwartz, M. Kumar, B.L. Adams, Electron Backscatter Diffraction in Materials Science, Kluwer Academic/Plenum Publishers, 2000.
[54] T.C. Isabell, V.P. Dravid, Ultramicroscopy 67 (1997) 59.
[55] Z. Wang, Z. Zhao, J. Qiu, J. Phys. Chem. Solids 69 (2008) 1296.
[56] F. Shi, Y. Song, J. Niu, X. Xia, Z. Wang, X. Zhang, Chem. Mater. 18 (2006) 1365.
[57] Y. Yang, G. Meng, J. Appl. Phys. 107 (2010) 044315.
[58] A. Gutes, C. Carraro, R. Maboudian, J. Am. Chem. Soc. 132 (2010) 1476.
[59] L. He, M. Lin, N. Kim, J. Raman Spectrosc. 41 (2010) 739.
[60] K.Q. Peng, J.J. Hu, Y.J. Yan, H. Fang, Y. Xu, S.T. Lee, S.T. Zhu, J., Adv. Funct. Mater. 16 (2006) 387.
[61] H. Lee, S. You, P.V. Pikhitsa, J. Kim, S. Kwon, Ch.-G. Woo, M Cho, Nano Lett. 11 (1) (2011) 119.